Journal of Solid State Chemistry 181 (2008) 1891–1898

Contents lists available at ScienceDirect

Journal of Solid State Chemistry

journal homepage: www.elsevier.com/locate/jssc

Lead–strontium borate halides with hilgardite-type structure and their SHG properties

B.V. Egorova [a], A.V. Olenev [b], P.S. Berdonosov [b,*], A.N. Kuznetsov [b], S.Yu. Stefanovich [b], V.A. Dolgikh [b], T. Mahenthirarajah [c], P. Lightfoot [c]

[a] Department of Materials Science, Moscow State University, Leninskie Gory, Moscow 119991, GSP-1 Russia
[b] Department of Chemistry, Moscow State University, Leninskie Gory, Moscow 119991, GSP-1 Russia
[c] EaStChem, School of Chemistry, St. Andrews University, St. Andrews, KY16 9ST, UK

ARTICLE INFO

Article history:
Received 18 February 2008
Received in revised form
7 April 2008
Accepted 19 April 2008
Available online 1 May 2008

Keywords:
Borates
Hilgardite
Nonlinear optics
Second harmonic generation
Crystal structure

ABSTRACT

Lead-containing members of the hilgardite family of borate halides, $M_2B_5O_9X$ (M = Ca, Sr, Ba, Pb; X = Cl, Br) exhibit an abnormally large nonlinear optical response. In order to establish any underlying crystal-chemical rationale for this we have carried out detailed crystallographic characterisations of the representative members of this series, $Sr_2B_5O_9Cl$ and $Pb_2B_5O_9Cl$, using powder neutron diffraction. Both adopt the orthorhombic hilgardite structure type, in space group *Pnn*2. The full solid solution range $Pb_{2-x}Sr_xB_5O_9Cl$ has also been prepared, and studied by X-ray Rietveld and second harmonic generation (SHG) measurements. The SHG response shows a linear decrease with increasing x, whereas the unit cell shows an increasing orthorhombic distortion. However, the crystallographic results suggest no significant or systematic changes in the nature of the borate sublattice between $Sr_2B_5O_9Cl$ and $Pb_2B_5O_9Cl$. We conclude that the enhanced SHG response in Pb-containing hilgardites is due predominantly to the presence of the polarizable nature of Pb^{2+}, in particular the presence of a stereochemically active lone pair.

1. Introduction

One of the fundamental objectives of modern functional materials science is the conversion of IR laser radiation into UV due to the second harmonic generation (SHG) effect. Crystals suitable for such a transformation should satisfy at least the following three criteria: (i) a wide range of optical transmittance for both the source and converted wavelength of radiation; (ii) a high damage threshold for a powerful laser beam and (iii) possess a high value of nonlinear optical (NLO) susceptibility of second order.

Concerning these requirements, many borates demonstrate unique optical characteristics in addition to laser radiation stability [1,2]. Therefore, borates are considered as the most promising class of materials for discovering new IR–UV converters. However, in most cases their SHG activity is weak compared to currently used optical materials such as potassium dihydrogen phosphate (KDP) or $LiNbO_3$ [1]. The discovery of high SHG activity in lead pentaborate bromide, $Pb_2B_5O_9Br$, rivalling these nonborate materials, is of key importance from both the applied and academic viewpoints.

$Pb_2B_5O_9Br$ has a crystal structure of the hilgardite type [3–5] consisting of a 3D framework of vertex-connected BO_4 tetrahedra and BO_3 triangles. Such a complex borate sublattice makes a theoretical description of the abnormal SHG activity of this compound difficult. In accordance with Philips–Van Vechten–Levine–Xue bond theory [6] the B–O bonds of planar BO_3 triangles make the main contribution to optical nonlinearities of hilgardites. However, this factor is not yet able to explain the very high SHG output from $Pb_2B_5O_9X$ (X = Cl, Br) hilgardites in comparison with their alkaline earth analogs [6].

One explanation that may be suggested is the so-called lone pair effect from Pb(II) ions [3–5], which the calculations presented in [6] neglect. To examine this lone pair influence it is instructive to study mixed cation derivatives among the hilgardite-type structures, in which the lead positions are partially occupied by alkaline earth cations. To the best of our knowledge there is no literature data about such compounds up to now.

In this study we report the detailed crystal structures of $Pb_2B_5O_9Cl$ and $Sr_2B_5O_9Cl$, the synthesis of some mixed $Pb_{2-x}Sr_xB_5O_9Cl$ phases, their structural characteristics and the results of SHG tests. The choice of strontium as substituting element was based on the similarity of the ionic radii of Sr^{2+} and Pb^{2+} ions (e.g. 1.31 and 1.35 Å, respectively for 9-coordination) [7], which should minimize cation size effects on the crystal structure

* Corresponding author. Fax: +7 495 939 0998.
E-mail address: berdonosov@inorg.chem.msu.ru (P.S. Berdonosov).

0022-4596/$ - see front matter © 2008 Elsevier Inc. All rights reserved.
doi:10.1016/j.jssc.2008.04.018

and SHG characteristics, allowing the lone pair influence to be studied directly.

2. Experimental

2.1. Sample preparation

The following reactions were used for $M_2B_5O_9Cl$ (M = Pb, Sr) preparation:

$$PbO + 2PbCl_2 + 5PbB_4O_7 \rightarrow 4Pb_2B_5O_9Cl \quad (1)$$

$$3SrO + SrCl_2 + 5B_2O_3 \rightarrow 2Sr_2B_5O_9Cl \quad (2)$$

or

$$3SrCO_3 + SrCl_2 + 10H_3BO_3 \rightarrow 2Sr_2B_5O_9Cl + 3CO_2 + 15H_2O \quad (3)$$

PbO, $PbCl_2$, $SrCO_3$, $SrCl_2 \cdot 6H_2O$, B_2O_3 were used of high grade purity. PbB_4O_7 was prepared from a PbO/H_3BO_3 mixture [8]. SrO was prepared by heating $SrCO_3$ at 1100 °C for 24 h. $SrCl_2 \cdot 6H_2O$ and B_2O_3 were preheated just before reaction mixture preparation.

Conditions of the $M_2B_5O_9Cl$ (M = Sr, Pb) syntheses for the X-ray and SHG measurements are shown in Table 1. The bulk samples for powder neutron diffraction (PND) experiments were prepared according to Schemes (1) and (3). Due to the high neutron absorption cross-section of naturally occurring boron, samples were prepared with 99% enriched $^{11}B_2O_3$ or $H_3{}^{11}BO_3$. Starting materials were pressed into pellets and after preheating of Sr sample with H_3BO_3 at 300 °C for 15 h the pellets were heated at higher temperatures (750 °C for 2 h for $Pb_2B_5O_9Cl$ and 650 °C for 3 h and 750 °C for 1.5 h with intermittent grindings for $Sr_2B_5O_9Cl$). After the heating the samples were quenched to room temperature by removing from the box furnace.

The mixed samples $Pb_{2-x}Sr_xB_5O_9Cl$ (x = 0.25, 0.5, 0.75, 1, 1.25, 1.5, 1.75) were prepared by the following reactions:

$$(1 - x/2)Pb_2B_5O_9Cl + x/2Sr_2B_5O_9Cl \rightarrow Pb_{2-x}Sr_xB_5O_9Cl; \quad (4)$$

$$3/2xSrCO_3 + 1/2xSrCl_2 \cdot 6H_2O + (3 - 3/2x)PbO + (1 - 1/2x)PbCl_2 + 10H_3BO_3 \rightarrow 2Pb_{2-x}Sr_xB_5O_9Cl + 3/2xCO_2\uparrow + (15 + 3x)H_2O. \quad (5)$$

The annealing conditions are listed in Table 1.

2.2. Powder neutron diffraction (PND) diagnostics

For $Pb_2B_5O_9Cl$ the PND was carried out on the GEM instrument at the ISIS facility, Rutherford Appleton Laboratory, UK. The ISIS neutron source operates in time-of-flight (energy-dispersive mode) so that data are analyzed as a function of d-spacing. The PND experiment on $Sr_2B_5O_9Cl$ was performed on the D2B high-resolution two-axis diffractometer at The ILL, Grenoble. The pattern was recorded in the 2θ range of 10–160° at a wavelength of 1.594 Å. The resulting Rietveld plots for PND are presented in Fig. 1. The crystallographic data and structure refinement details for $Pb_2B_5O_9Cl$ and $Sr_2B_5O_9Cl$ are listed in Tables 2 and 3, and salient bond lengths in Table 4.

2.3. X-ray diagnostics

All the samples were tested by X-ray diffraction recorded in a Guinier camera (FR-552, Cu $K\alpha1$) using germanium as an internal standard, or using a Stoe STADI/P diffractometer operating in transmission mode, equipped with a linear position-sensitive

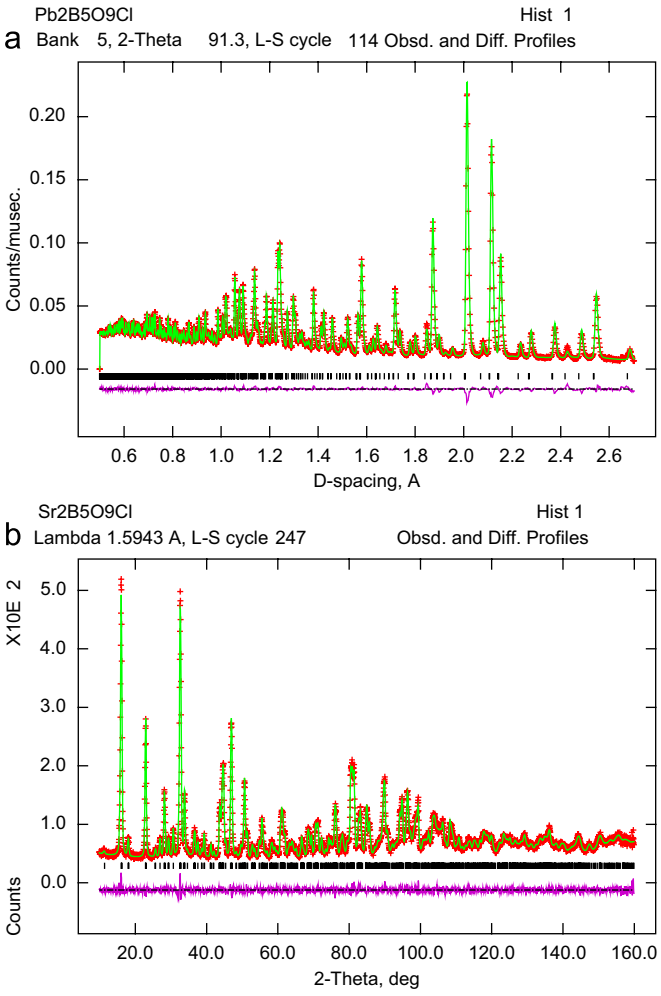

Fig. 1. Rietveld fits for PND experiments on $Pb_2B_5O_9Cl$ (a) and $Sr_2B_5O_9Cl$ (b).

Table 1
Conditions of synthesis of the $M_2B_5O_9Cl$ (M = Sr, Pb) and $Pb_{2-x}Sr_xB_5O_9Cl$ (x = 0.25, 0.5, 0.75, 1, 1.25, 1.5, 1.75)

Phase	Starting charge	Container	Annealing conditions
$Pb_2B_5O_9Cl$	PbO $2PbCl_2$ $5PbB_4O_7$	Alumina crucible	450 °C (60 h); grinding; 700 °C (120 h)
$Sr_2B_5O_9Cl$	3SrO $SrCl_2$ $5B_2O_3$	Alumina crucible in evacuated quartz ampoule	950 °C (60 h); cooling (0.5 °C/h) till 900 °C, cooling (5 °C/h) till 700 °C
$Pb_{2-x}Sr_xB_5O_9Cl$	$(1-x/2)Pb_2B_5O_9Cl$ $x/2$ $Sr_2B_5O_9Cl$	Alumina crucible in evacuated quartz ampoule	600 °C (60 h)
$Pb_{2-x}Sr_xB_5O_9Cl$	$(3/2x)SrCO_3$ $(1/2x)SrCl_2 \cdot 6H_2O$. $(3-3/2x)PbO$ $(1-1/2x)PbCl_2$ $10H_3BO_3$	Alumina crucible	(I) 700 °C (120 h), grounding, reheating three times; cooling in the switched off furnace; (II) 700 °C (120 h), quenching

Table 2
Crystal data and structure refinement for $Pb_2B_5O_9Cl$ and $Sr_2B_5O_9Cl$ from PND

Formula	$Pb_2B_5O_9Cl$	$Sr_2B_5O_9Cl$
Instrument	GEM (ISIS)	D2B (ILL)
Temperature	293(2)	293(2)
Crystal system	Orthorhombic	Orthorhombic
Space group	*Pnn*2 (34)	*Pnn*2 (34)
Unit cell dimensions (A)		
a	11.3810(3)	11.3153(5)
b	11.3840(3)	11.3838(5)
c	6.56335(12)	6.4945(2)
Volume (A^3)	850.36(3)	836.57(7)
Z	4	4
Density (calculated) (mg/m^3)	5.060	3.245
Refinement method	Rietveld refinement	Rietveld refinement
Refinement software	GSAS [10]	GSAS [10]
Number of parameters	137	100
Goodness-of-fit	2.70	1.36
*R*p	0.0212	0.0315
*R*wp	0.0208	0.0388

Table 3
Atomic coordinates and isotropic thermal parameters for $Pb_2B_5O_9Cl$ and $Sr_2B_5O_9Cl$

Atom	Site	*x*	*y*	*z*	U_{iso}, $Å^2$
$Pb_2B_5O_9Cl$					
Pb1	4*c*	0.0397(3)	0.2523(3)	0.0001(4)	0.0075(3)
Pb2	4*c*	0.2405(2)	0.0219(2)	−0.6674(5)	0.0075(3)
Cl1	2*a*	0	0	−0.8782(7)	0.0051(4)
Cl2	2*b*	1/2	0	−0.6187(6)	0.0051(4)
O1	4*c*	0.3184(4)	0.2387(3)	−0.5814(6)	0.00600(18)
O2	4*c*	0.4271(3)	0.2126(4)	−0.1731(7)	0.00600(18)
O3	4*c*	0.2256(4)	0.2717(4)	−0.2463(7)	0.00600(18)
O4	4*c*	0.2748(4)	0.0720(4)	−0.2474(6)	0.00600(18)
O5	4*c*	0.4481(3)	0.2863(4)	−0.8392(6)	0.00600(18)
O6	4*c*	0.2605(3)	0.3808(4)	−0.8375(6)	0.00600(18)
O7	4*c*	0.2739(4)	0.1803(4)	−0.9302(6)	0.00600(18)
O8	4*c*	0.2104(4)	0.4192(3)	−0.4935(6)	0.00600(18)
O9	4*c*	0.1157(4)	0.2321(4)	−0.5613(6)	0.00600(18)
B1	4*c*	0.3221(3)	0.2712(3)	−0.7966(5)	0.00253(17)
B2	4*c*	0.3015(3)	0.1816(3)	−0.1453(5)	0.00253(17)
B3	4*c*	0.2173(3)	0.2889(3)	−0.4656(5)	0.00253(17)
B4	4*c*	0.2307(3)	0.4588(3)	−0.6912(5)	0.00253(17)
B5	4*c*	0.4988(3)	0.2538(3)	−0.0232(6)	0.00253(17)
$Sr_2B_5O_9Cl$					
Sr1	4*c*	0.0456(6)	0.2511(8)	0.0088(11)	0.0134(10)
Sr2	4*c*	0.2408(6)	0.0272(7)	−0.6561(11)	0.0134(10)
Cl1	2*a*	0	0	−0.8554(16)	0.0225(11)
Cl2	2*b*	1/2	0	−0.5997(15)	0.0225(11)
O1	4*c*	0.3153(7)	0.2444(7)	−0.5829(12)	0.0075(6)
O2	4*c*	0.4229(7)	0.2131(7)	−0.1769(14)	0.0075(6)
O3	4*c*	0.2239(7)	0.2807(6)	−0.2495(14)	0.0075(6)
O4	4*c*	0.2651(7)	0.0789(6)	−0.2507(11)	0.0075(6)
O5	4*c*	0.4495(6)	0.2804(7)	−0.8413(13)	0.0075(6)
O6	4*c*	0.2656(6)	0.3867(7)	−0.8500(12)	0.0075(6)
O6	4*c*	0.2648(7)	0.1824(8)	−0.9302(13)	0.0075(6)
O8	4*c*	0.2051(8)	0.4232(7)	−0.5027(11)	0.0075(6)
O9	4*c*	0.1118(7)	0.2346(8)	−0.5769(11)	0.0075(6)
B1	4*c*	0.3210(6)	0.2711(6)	−0.7937(10)	0.0046(6)
B2	4*c*	0.2937(6)	0.1889(6)	−0.1497(11)	0.0046(6)
B3	4*c*	0.2135(6)	0.2947(6)	−0.4719(11)	0.0046(6)
B4	4*c*	0.2360(6)	0.4629(5)	−0.6901(10)	0.0046(6)
B5	4*c*	0.4929(6)	0.2516(7)	−0.0270(11)	0.0046(6)

detector. For the Guinier data, line positions on the films were measured with an accuracy of ca. 5 μm, and converted into interplanar spacings using a home-made program "Powder 2". ICDD PDF-2 [9] was used for phase identification. For the mixed compositions $Pb_{2-x}Sr_xB_5O_9Cl$ with $x = 1$, 1.5 and 1.75 Rietveld refinement was performed on the X-ray data in order to determine precise cell constants and to estimate the distribution

Table 4
Interatomic distances for $Pb_2B_5O_9Cl$ and $Sr_2B_5O_9Cl$ (Å)

$Pb_2B_5O_9Cl$		$Sr_2B_5O_9Cl$	
Bond	Distance	Bond	Distance
Pb1–Cl1	3.015(3)	Sr1–Cl1	3.036(9)
Pb1–Cl2	2.961(3)	Sr1–Cl2	2.965(9)
Pb1–O1	2.577(5)	Sr1–O1	2.674(10)
Pb1–O2	2.530(5)	Sr1–O2	2.503(10)
Pb1–O3	2.672(6)	Sr1–O3	2.645(11)
Pb1–O5	2.497(5)	Sr1–O5	2.546(11)
Pb1–O6	3.097(5)	Sr1–O6	3.069(10)
Pb1–O7	2.826(6)	Sr1–O7	2.630(11)
Pb1–O9	3.015(5)	Sr1–O9	2.799(10)
Pb2–Cl1	3.078(3)	Sr2–Cl1	3.033(8)
Pb2–Cl2	2.981(2)	Sr2–Cl2	2.972(7)
Pb2–O1	2.683(5)	Sr2–O1	2.655(11)
Pb2–O3	2.920(5)	Sr2–O3	2.899(11)
Pb2–O4	2.842(5)	Sr2–O4	2.711(11)
Pb2–O6	2.696(5)	Sr2–O6	2.553(12)
Pb2–O7	2.524(5)	Sr2–O7	2.523(12)
Pb2–O8	2.502(5)	Sr2–O8	2.617(11)
Pb2–O9	2.869(5)	Sr2–O9	2.823(10)
B1–O1	1.461(5)	B1–O1	1.404(10)
B1–O5	1.472(5)	B1–O5	1.489(10)
B1–O6	1.456(5)	B1–O6	1.503(9)
B1–O7	1.463(5)	B1–O7	1.487(11)
B2–O2	1.484(5)	B2–O2	1.498(9)
B2–O3	1.497(5)	B2–O3	1.462(10)
B2–O4	1.449(6)	B2–O4	1.450(10)
B2–O7	1.446(6)	B2–O7	1.464(12)
B3–O1	1.493(6)	B3–O1	1.474(11)
B3–O3	1.456(5)	B3–O3	1.458(10)
B3–O8	1.497(5)	B3–O8	1.479(10)
B3–O9	1.465(5)	B3–O9	1.503(10)
B4–O4	1.342(6)	B4–O4	1.378(9)
B4–O6	1.351(5)	B4–O6	1.394(11)
B4–O8	1.393(5)	B4–O8	1.344(10)
B5–O2	1.361(6)	B5–O2	1.329(12)
B5–O5	1.389(6)	B5–O5	1.343(11)
B5–O9	1.364(5)	B5–O9	1.392(10)

Table 5
Crystallographic parameters for $Pb_{2-x}Sr_xB_5O_9Cl$ $x = 1$, 1.5 and 1.75

x	1	1.5	1.75
Instrument		Stoe STADI P	
X-ray		Cu*K*α1	
Temperature		293(2)	
Crystal system		Orthorhombic	
Space group		P n n 2 (34)	
Unit cell dimensions (A)			
a	11.34291(13)	11.33297(16)	11.32657(13)
b	11.37535(13)	11.38335(16)	11.38146(13)
c	6.52615(7)	6.51118(9)	6.50281(7)
Volume (A^3)	842.066(18)	839.988(26)	838.296(22)
Z		4	
Refinement method		Rietveld Refinement	
Refinement software		GSAS [10]	
Number of parameters	34	34	34
Goodness-of-fit	1.63	2.11	1.87
*M*1 site occupancy			
Sr	0.630(7)	0.750(6)	0.868(4)
Pb	0.370(7)	0.250(6)	0.132(4)
*M*2 site occupancy			
Sr	0.576(7)	0.749(6)	0.855(4)
Pb	0.424(7)	0.251(6)	0.145(4)
*R*p	0.0480	0.0479	0.0464
*R*wp	0.0669	0.0673	0.0607

of the metal ions on the two discrete cation positions. X-ray patterns in range of 10–110° 2Θ with step size 0.01° were collected on a Stoe STADI P diffractometer, and data analysis was

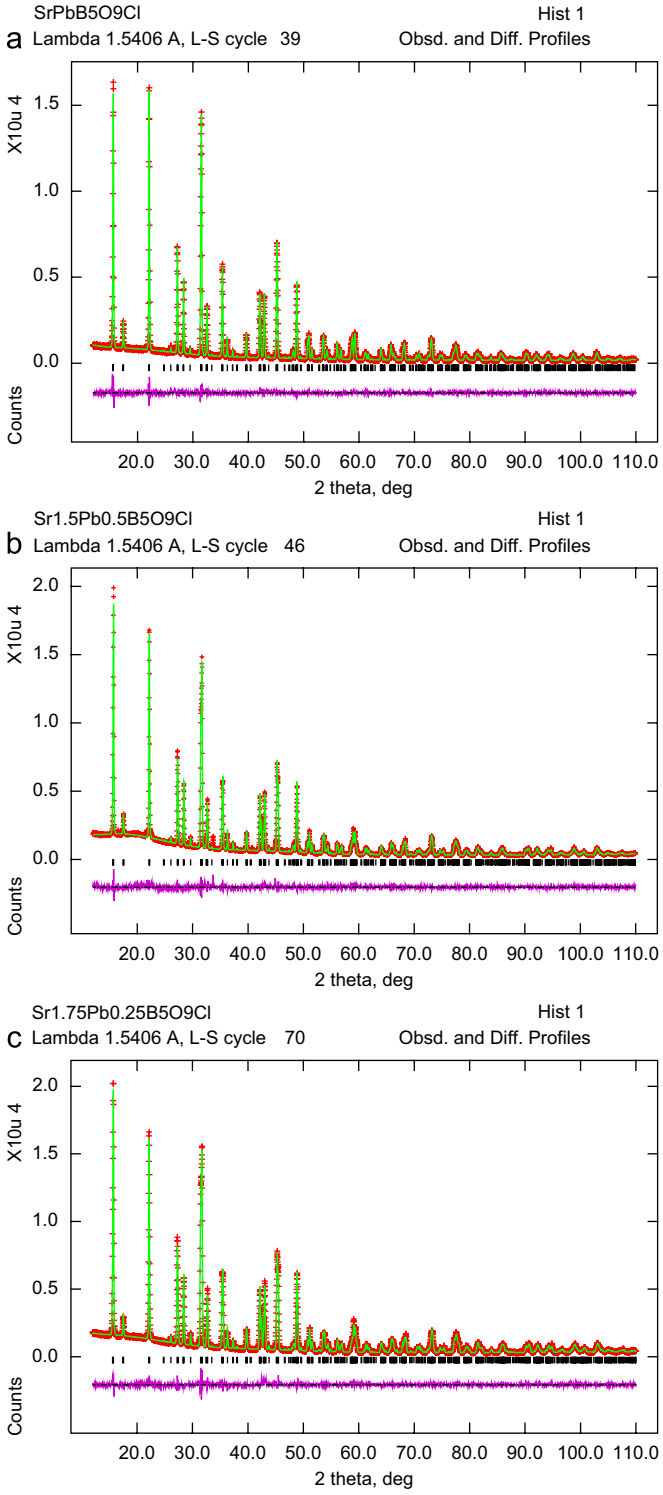

Fig. 2. Final Rietveld fits for the X-ray experiments for $Pb_{2-x}Sr_xB_5O_9Cl$, $x = 1$ (a), 1.5 (b) and 1.75 (c).

carried out using the GSAS software [10]. The positions of oxygen and boron atoms were not refined. The results of refinement are presented in Table 5 and Fig. 2. The site occupancies for *M*1 and *M*2 metal sites were refined with the constraints that each site is fully occupied and all the isotropic thermal parameters are equivalent. Further details (CIF files) may be found in the Supplementary data.

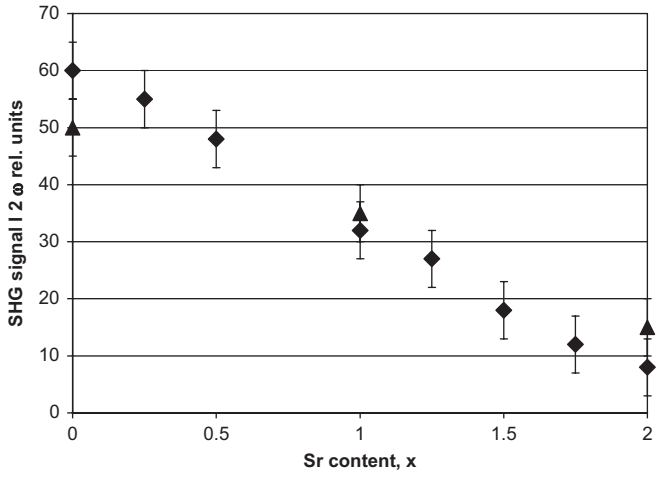

Fig. 3. The dependence of SHG values for different $Pb_{2-x}Sr_xB_5O_9Cl$ compositions relative to 3-μm powder α-quartz standard. Diamonds and triangles stand for samples with the same composition from the different series of syntheses.

2.4. SHG measurements

The NLO properties of the series $Pb_{2-x}Sr_xB_5O_9Cl$ ($x = 0$; 0.25, 0.5, 0.75, 1, 1.25, 1.5, 1.75, 2) were studied by the powder SHG technique, with the set-up similar to that employed by Kurtz and Perry [11]. Graded powder samples were sieved into fractions according to particle size. A YAG:Nd-laser was used as a source of powerful pulsed radiation at wavelength $\lambda = 1.064\,\mu m$ with a repetition rate of 4 pulses per second and a pulse duration of about 10 ns. The intensities $I_{2\omega}$ of the signals at doubled frequency ($\lambda_{2\omega} = 0.532\,\mu m$) were registered from substances in reflection mode. The measured values are presented in Fig. 3, relative to the SHG intensity of a standard 3-μm α-quartz powder. The different intensities for the same *x* values correspond to different series of samples obtained from different syntheses.

2.5. Quantum chemical procedures

First-principles electronic structure calculations on the periodic structure of $Pb_2B_5O_9Cl$ were performed on the density functional theory level using a hybrid density functional (B3LYP), employing the CRYSTAL98 program [12]. All calculations included a converged SCF run, with the convergence threshold set at 10^{-7}. Hay and Wadt, large-core (HAYWLC) pseudopotentials were applied to the chlorine and lead atoms and the original Hay and Wadt valence basis sets of double-zeta quality were used as given in Ref. [13]. For the boron and oxygen atoms, all-electron split-valence 6-21G basis sets were used.

Electron localization function (ELF) distribution $\eta(r)$ was calculated using the TOPOND98 program [14] based on the results of the SCF calculations. The topology of the ELF surface was investigated using the gOpenMol package [15].

3. Results and discussion

NLO susceptibility is very sensitive to the type and length of chemical bonds in the crystal structure. In the case of borates, the relative orientations of the polarizable borate groups are deemed to be a significant factor [1,16]. However, based on a comparison of the boron–oxygen framework in the structures of well-characterised hilgardites (published single-crystal X-ray refinements of $Ca_2B_5O_9Br$ [17], $Ba_2B_5O_9Cl$ [18] and $Pb_2B_5O_9Br$

[3–5], together with our own PND data on $Ba_2B_5O_9Cl$, $Pb_2B_5O_9Br$, $Pb_2B_5O_9Cl$ and $Sr_2B_5O_9Cl$) the B–O framework is not dramatically or systematically changed as a function of composition. The abnormally high SHG signal from the lead-containing compounds may therefore be considered to be a result of the local environment of the lead atoms in the crystal structure, in particular the influence of the lone electron pair of the Pb^{2+} ions. Until now there has been no precise structural data for $Pb_2B_5O_9Cl$ and $Sr_2B_5O_9Cl$ in the literature and these data are presented in our work.

The neutron diffraction data (Table 2) were treated within the structure model described in [3–5,17] for the bromine analogues, leading to a more precise determination of the light atom positions (Table 3); typical precision on the B–O bond lengths from our PND is in the range ± 0.005–0.010 Å, as compared to ± 0.02 and ± 0.03 Å for the single-crystal X-ray studies in Refs. [5,13]. Further discussion is based on the PND solutions.

Crystallographic data for $M_2B_5O_9Cl$ (M = Sr, Pb) are presented in Tables 2–4. In early works, the crystal structures of $Pb_2B_5O_9Cl$ [19] and $Sr_2B_5O_9Cl$ [20] were considered as tetragonal with cell parameters $a = 11.32$, $c = 6.53$ Å and $a = 11.35$, $c = 6.50$ Å, respectively. Later work has concluded that each of the anhydrous hilgardites has orthorhombic symmetry, space group *Pnn*2, so it may be noted that the crystal structures have a pronounced pseudo-tetragonal character, especially marked for $Pb_2B_5O_9Cl$, although there is no crystallographically imposed four-fold symmetry.

The crystal structure of $M_2B_5O_9Cl$ (M = Pb, Sr) is represented in Fig. 4. The basis of the structure is a boron–oxygen framework formed from five crystallographically independent borate groups; two BO_3 triangles and three BO_4 tetrahedra, which are linked into a $[B_5O_9]^{3-}$ fundamental building block. The tetrahedra are connected to each other by common vertices to form infinite chains along the *c*-axis of the unit cell. Such chains are connected in perpendicular directions by means of the BO_3 triangles. The resulting 3D framework contains channels where the metal ions and chloride ions are situated. The B–O bond distances lie in the range typical for triangular and tetrahedral borate groups (Table 4).

The crystal structure contains two crystallographically independent cation positions (Table 3). In $Pb_2B_5O_9Cl$ the coordination environment of both lead atoms may be described as a very distorted hexagonal bipyramid, formed by six oxygen atoms in the base and two chlorine atoms at the vertices. Bond valence sum calculations [21] allow us to exclude the longest Pb1–O6 distance: 3.097(5) Å (Table 4) from the coordination sphere. Thus, the surrounding of Pb1 may be described as $Pb1O_{4+2}Cl_2$, with four oxygen atoms in the range 2.497(5)–2.672(6) Å and two at a longer distance 2.826(6)–3.015(5) Å (Fig. 5a). Cl2 and the four closest oxygens form an umbrella-like environment of Pb1 and the other oxygen atoms and Cl1 are situated on the other side of this umbrella. A similar situation takes place for the Pb2 environment: four oxygen atoms situated at short distances 2.502(2)–2.696(5) Å and two chlorine atoms at 2.981(2)–3.078(3) Å. In this case, there are three other oxygen atoms surrounding Pb2 at distances in the range 2.842(5)–2.920(5) Å (Fig. 5b). Thus the Pb2 polyhedron may be described as a hexagonal bipyramid capped by one oxygen atom. As shown in Fig. 5 both lead atoms are shifted from the equatorial planes (oxygen hexagons) of the bipyramids. Usually [3–5] this phenomenon is considered as a stereochemically active lone electron pair effect. In this case the location of the lone pair for the two different lead ions will be different and there should be different stereochemical activity for the two different sites. We could not determine the electron pair positions from our PND data, but based on the suggested crystallographic model the contribution to the summed NLO susceptibility will be different for the Pb1 and Pb2 atoms. For $Sr_2B_5O_9Cl$ similar polyhedra may be described (Table 4).

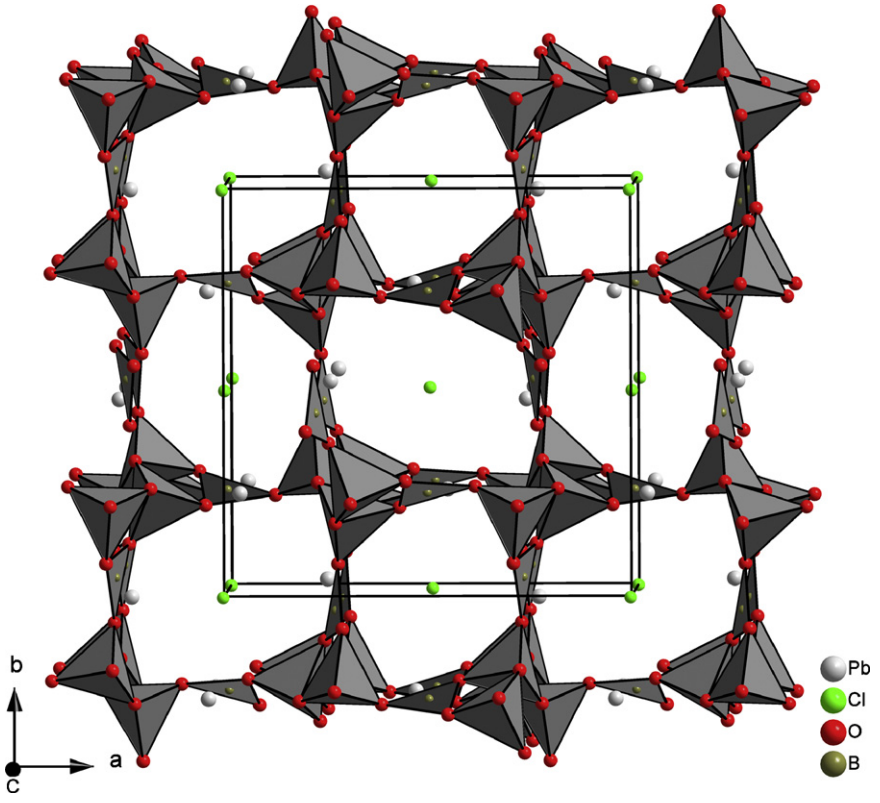

Fig. 4. The crystal structure of $Pb_2B_5O_9Cl$. The boron–oxygen framework and the unit cell are shown.

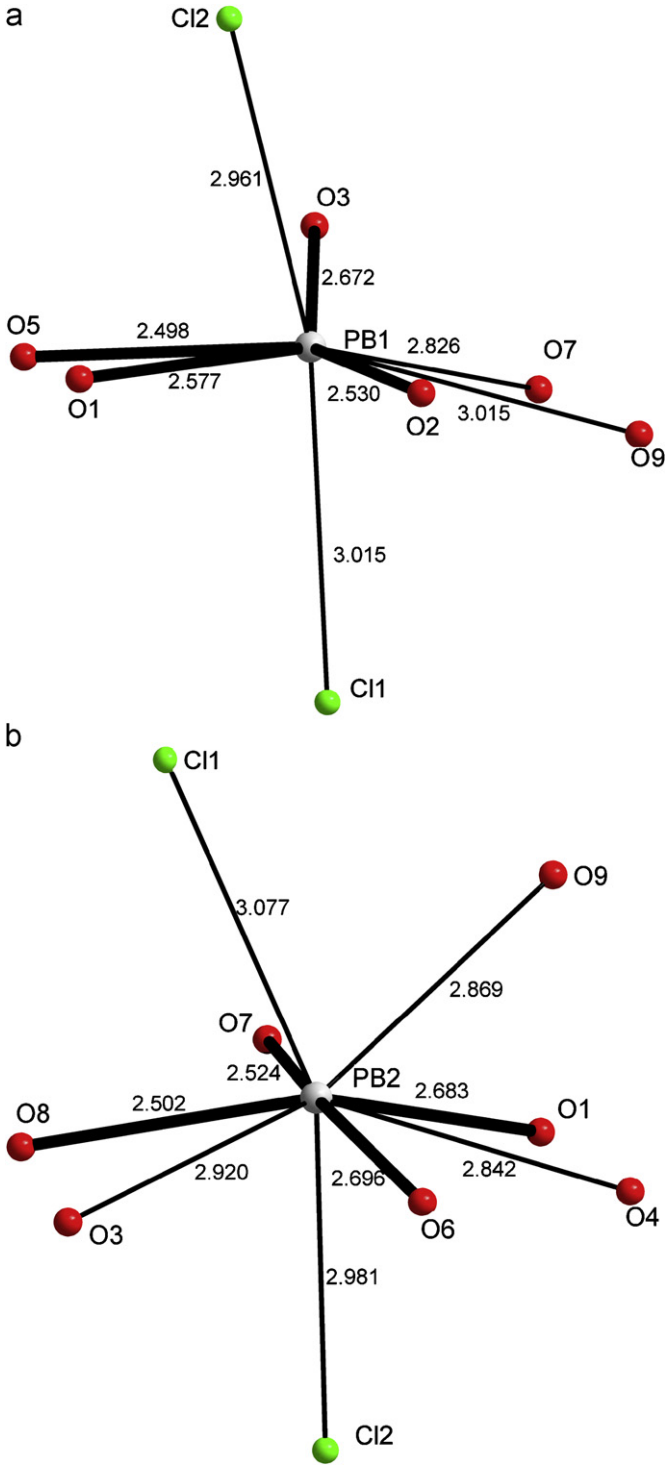

Fig. 5. The coordination environment of Pb1(a) and Pb2(b) in the crystal structure of $Pb_2B_5O_9Cl$. Shortest Pb–O bonds of the primary coordination sphere are drawn as thick lines.

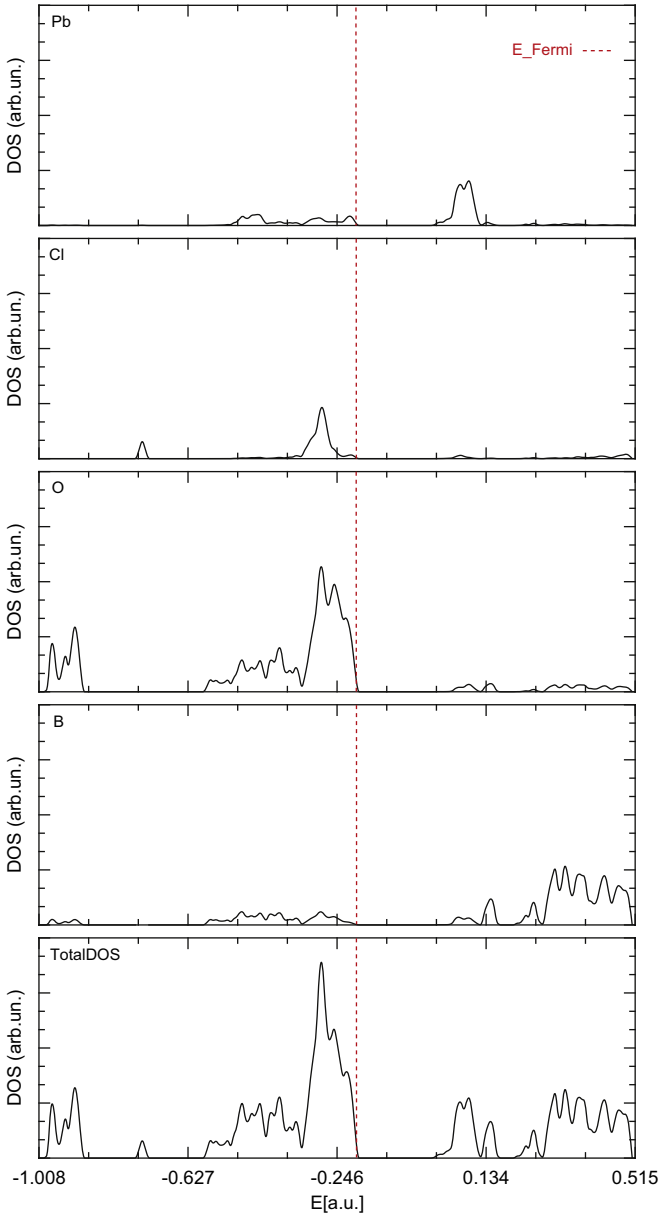

Fig. 6. Calculated total and projected DOS for the $Pb_2B_5O_9Cl$ structure.

First-principles calculations of electronic structure for $Pb_2B_5O_9Cl$ predict the compound to exhibit semiconducting behavior (Fig. 6). The major contribution to the valence band near the Fermi level is provided by oxygen and chlorine atoms, while lead states are dominant in the conduction band. Nevertheless, as seen from Fig. 6, boron and lead contributions to the valence band are in the same energy range as those from the oxygen. Calculated Mulliken charges are: Pb—ca. +1.32, Cl—ca. −0.79, O—ca. −0.70, B—ca. +0.89. Such charge distribution is in good agreement with the interpretation of interactions between the boron–oxygen framework and Pb and Cl atoms in the channels as sufficiently ionic.

In order to gain more insight into the peculiarities of the structure of $Pb_2B_5O_9Cl$ and the possibility of the lone pair influence, we have investigated the topology of ELF (Fig. 7). At the high η values, corresponding to a high degree of electron localization, the most prominent features are the regions around the lead atoms, evidently corresponding to the 6*s*-pairs. As we lower the η value, other features arise, such as boron–oxygen pairwise interactions and oxygen localized 2*p*-electrons, clearly visible at $\eta = 0.85$. For us, however, the objects of most interest are the lead lone pairs. Our ELF calculations show that they are arranged mostly in the *ab* plane and nonsymmetrical with respect to the Pb atoms. Such an asymmetric distribution may be considered as a display of stereochemical activity and be associated with the distortion in the coordination of Pb atoms. The distribution of the pairs around Pb1 and Pb2 atoms is quite

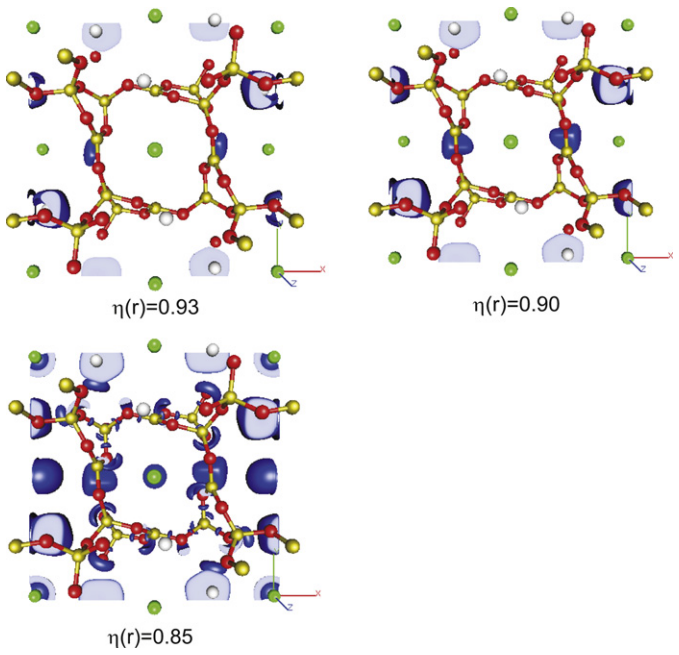

Fig. 7. The ELF isosurfaces for the $Pb_2B_5O_9Cl$ structure.

similar, the difference being only the direction of the asymmetric shift: along the *b*-axis for Pb1 atoms and along the *a*-axis for Pb2.

It has to be noted that the topology of the ELF can be basis-sensitive. Moreover, ECP-based basis sets can be safely used only for the cases when the valence states are well-separated from the core states. While this has been proven viable for such heavy elements as Pb or Bi [22], which justifies our analysis of electron localization on lead atoms, we nevertheless consider only the qualitative results of our investigation. A thorough analysis of the ELF topology over the unit cell of the $Pb_2B_5O_9Cl$ requires a special investigation with more computational effort.

From the NLO susceptibility point of view the distribution of two different atoms with and without lone electron pairs within two crystallographic sites is very important. In order to reveal any order or disorder character of this distribution, the mixed Pb/Sr compounds were studied.

In the series $Pb_{2-x}Sr_xB_5O_9Cl$ (Table 1) the final product phase was identified as hilgardite-like, for all values of *x*. Their powder patterns were practically fully indexed in the orthorhombic cell anticipated for anhydrous hilgardite, besides one or two weak impurity reflections. Rietveld refinement from X-ray powder diffraction data was performed for $x = 1$, 1.5 and 1.75 (Table 5, Fig. 2). Refinement of the composition of each cation site shows that the actual compositions are slightly shifted from the ideal compositions, but in the context of our investigation the difference in the *M*1 and *M*2 site occupancies is the most interesting parameter, which may reveal a slightly preferred occupation of one or another site by strontium or lead atoms. In Fig. 8 the dependence of cell parameters on composition is presented, together with data from the PND refinements. It is clear that the cell parameters *a* and *c*, as well as the cell volume, decrease with increasing strontium content, whereas the *b* cell constant remains fairly constant, except for a distinct 'dip' around $x = 1$. Overall, there is a consequent increase in the degree of orthorhombic distortion with increasing Sr content. The anomalous behavior near $x = 1$ may correspond to some kind of ordering in the Sr and Pb distribution on the *M*1 and *M*2 sites. Attempts to refine site occupancies for the *M*1 and *M*2 sites shows (Table 5) that for compositions $x = 1.5$ and 1.75 the Sr/Pb

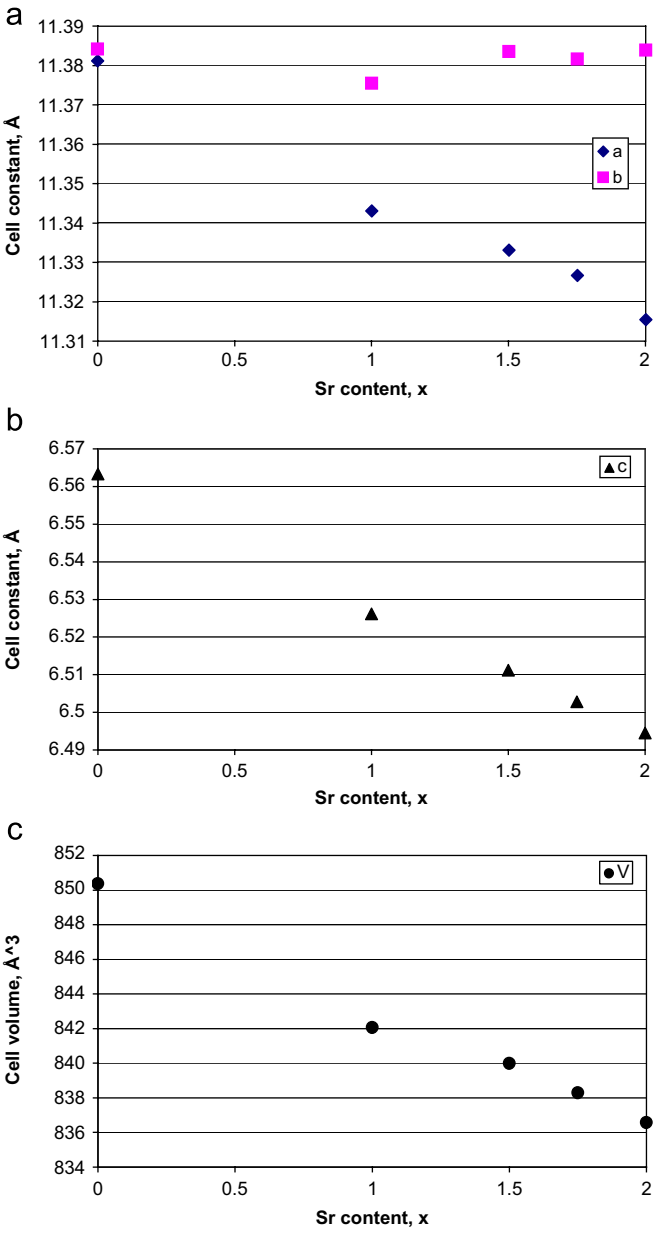

Fig. 8. Variation of cell constants with Sr content for $Pb_{2-x}Sr_xB_5O_9Cl$.

distribution is statistical. For $x = 1$ we may tentatively suggest some level of ordering, whereby Sr shows a preference for the *M*1 site rather than *M*2. This result may suggest the existence of an ordered compound with $x \approx 1$ as occurs for hydrated $CaSr(B_5O_9)Cl \cdot H_2O$ (triclinic hylgardite type 1A) where Ca and Sr are situated in different sites [23].

The SHG measurements (Fig. 3) across the series $Pb_{2-x}Sr_xB_5O_9Cl$ show a clear linear decrease of SHG signal intensity ($I_{2\omega}$) as a function of increasing *x*. From the data presented it may be concluded that, within errors, the SHG response does not deviate from a linear dependence with Sr content. It may be suggested that the most significant impact on SHG intensity is the Pb content in the compound, and the abnormally high SHG intensity in the Pb-containing hilgardites is an effect of the lone electron pairs from Pb^{2+} ions in both crystallographic sites, rather than any significant effect from cation-induced modifications of the borate sublattice.

Acknowledgments

We thank Dr. R.I. Smith for collection of the neutron diffraction data at ISIS and Dr. R.J. Goff for assistance in the data collection at ILL. The Russian team thanks RFBR Project 06-03-32134 for financial support. PSB thanks INTAS for support through the Grant YS 05-109-4474.

Appendix A. Supporting material

Supplementary data associated with this article can be found in the online version at doi:10.1016/j.jssc.2008.04.018.

References

[1] P. Becker, Adv. Mater. 10 (1998) 979–992.
[2] T. Sasaki, Y. Mori, M. Yoshimura, Y.K. Yap, T. Kamimura, Mater. Sci. Eng. 30 (2000) 1–57.
[3] E.L. Belokoneva, Yu.K. Kabalov, O.V. Dmitriev, S.Yu. Stefanovich, Cryst. Rep. 48 (2003) 44–48.
[4] O.V. Yakubovich, N.N. Mochenova, O.V. Dimitrova, W. Massa, Acta Crystallogr. E 60 (2004) i127.
[5] E.L. Belokoneva, A.G. Al-Ama, S.Yu. Stefanovich, P.A. Plachinda, Cryst. Rep. 52 (2007) 795–800.
[6] P.A. Plachinda, V.A. Dolgikh, S.Yu. Stefanovich, P.S. Berdonosov, Solid State Sci. 7 (2005) 1194–1200.
[7] R.D. Shannon, Acta Crystallogr. A 32 (1976) 751–767.
[8] K.S. Bartwal, R. Bhatt, S. Kar, V.K. Wadhawan, Mater. Sci. Eng. B 85 (2001) 76–79.
[9] The International Centre for Diffraction Data 12 Campus Boulevard Newtown Square, PA 19073-3273 USA http://www.icdd.com PDF2 2001.
[10] A.C. Larson, R.B. Von Dreele, General Structure Analysis System (GSAS), Los Alamos National Laboratory Report LAUR 86-748 (2004).
[11] S.K. Kurtz, T.T. Perry, J. Appl. Phys. 39 (1968) 3798–3813.
[12] (a) C. Pisani, R. Dovesi, C. Roetti, HF Ab-Initio Treatment of Crystalline Systems. Lecture Notes in Chemistry, vol. 48, Springer, Berlin, 1988;
(b) V.R. Saunders, R. Dovesi, C. Roetti, M. Causa, N.M. Harrison, R. Orlando, C.M. Zicovich-Wilson, CRYSTAL98, University of Torino, Torino, 1998.
[13] P.J. Hay, W.R. Wadt, J. Chem. Phys. 82 (1985) 284–298.
[14] C. Gatti, TOPOND98 User's Manual, CNR-CSRSRC, Milano, 1999.
[15] (a) L. Laaksonen, J. Mol. Graphics 10 (1992) 33–34;
(b) D.L. Bergman, L. Laaksonen, A. Laaksonen, J. Mol. Graphics Model. 15 (1997) 301–306.
[16] C. Chen, Z. Lin, Z. Wang, Appl. Phys. B 80 (2005) 1–25.
[17] D.J. Lloyd, A. Levasseur, C. Fouassier, J. Solid State Chem. 6 (1973) 179–186.
[18] P. Held, J. Liebertz, L. Bohaty, Z. Kristallogr.-NCS 217 (2002) 463–464.
[19] C. Fouassier, A. Levasseur, P. Hagenmuller, J. Solid State Chem. 3 (1971) 206–208.
[20] T.E. Peters, J. Baglio, J. Inorg. Nucl. Chem. 32 (1970) 1089–1095.
[21] I.D. Brown, Bond valence sum parameters version 2006-05-02, http://www.ccp14.ac.uk/ccp/web-mirrors/i_d_brown/bond_valence_param/bvparm2006.cif.
[22] A.N. Kuznetsov, L. Kloo, M. Lindsjo, J. Rosdahl, H. Stoll, Chem. Eur. J. 7 (2001) 2821–2828.
[23] O. Ferro, D. Yu. Pushcharovski, S. Teat, S.A. Vinogradova, E.V. Lovskaya, I.V. Pekov, Cryst. Rep. 45 (2000) 410–415.